

# Temperature and composition dependence of the energy gap of $\text{Hg}_{1-x}\text{Cd}_x\text{Te}$ by two-photon magnetoabsorption techniques

D. G. Seiler and J. R. Lowney

*Semiconductor Electronics Division, National Institute of Standards & Technology, Gaithersburg, Maryland 20899*

C. L. Littler

*Department of Physics, University of North Texas, Denton, Texas 76203*

M. R. Loloee

*Department of Physics and Astronomy, Center for Fundamental Materials Research, Michigan State University, East Lansing, Michigan 48824*

(Received 4 October 1989; accepted 29 October 1989)

Accurate determinations of the energy gap  $E_g$  at liquid helium temperatures in alloys of  $0.24 \leq x \leq 0.30$  have been made by two-photon magnetoabsorption techniques. They are shown to help verify the use of the Hansen-Schmit-Casselmann (HSC) relation over the range  $0 < x < 0.30$  at these temperatures. In contrast, the observed temperature dependence of  $E_g$  below 77 K is nonlinear and thus cannot be described accurately by the HSC relation. Analysis of  $E_g(T)$  data for three samples with  $0.24 \leq x \leq 0.26$  has allowed the deduction of a new relationship for  $E_g(x, T)$  that more properly accounts for the nonlinear temperature dependence below 77 K and the linear behavior above 77 K, while still accurately describing the  $x$  dependence  $E_g(x, T) = -0.302 + 1.93x + 5.35(1 - 2x)(10^{-4})[(-1822 + T^3)/(255.2 + T^2)] - 0.810x^2 + 0.832x^3$ , for  $E_g$  in eV and  $T$  in K. This relation should apply to alloys with  $0.2 < x < 0.3$ . The maximum change from the HSC relation in this range is 0.004 eV for  $x = 0.2$  at  $\sim 10$  K.

## I. INTRODUCTION

Infrared detectors fabricated from mercury cadmium telluride (MCT or  $\text{Hg}_{1-x}\text{Cd}_x\text{Te}$ ) alloys are extremely important components of modern infrared systems. The primary parameter controlling the wavelength range for these intrinsic detectors is the fundamental energy gap  $E_g$ , defined as the energy difference between the conduction and valence bands. The exact value of  $E_g$  depends quite critically upon the value of the mole fraction of cadmium ( $x$ ) and the lattice temperature  $T$ . Numerous studies have thus been carried out by various authors over the last two decades to determine an accurate empirical relationship  $E_g(x, T)$  that properly predicts how  $E_g$  depends upon the mole fraction and the temperature.<sup>1-11</sup> Unfortunately, there is still considerable disagreement among the many different authors and no universally accepted relationship for  $E_g(x, T)$  exists. In this paper we resolve this controversy for  $0 \leq x \leq 0.3$  by using the results of two-photon magneto-optical measurements for various values of  $x$ . In addition, the nonlinear temperature dependence of  $E_g$  observed at low temperatures ( $T < 77$  K) is analyzed and incorporated into a new empirical relationship for  $E_g(x, T)$ . We note that the 8–12 and 3–5  $\mu\text{m}$  wavelength regions are very important since the majority of MCT infrared detectors are based upon material with  $x \approx 0.2$  and  $x \approx 0.3$ .

The most frequent methods for determining the MCT energy gap are based on either detector cutoff wavelength or optical absorption cuton. However, the definition of the energy gap from these types of measurements is ambiguous. The absorption edge is not infinitely sharp because of free carrier and phonon absorption along with band tailing ef-

fects. An example of the variability of defining  $E_g$  from an optical absorption measurement is (1) using the photon energy value<sup>2</sup> at which  $\alpha = 500 \text{ cm}^{-1}$ , as opposed to (2) using the energy at the turning point where the sharply rising region of the absorption curve crosses the comparatively smooth region of intrinsic absorption (usually observed for  $\alpha = 3000\text{--}4000 \text{ cm}^{-1}$ ).<sup>9</sup>

Photoluminescence experiments have also proven difficult to perform in the smaller band gap materials.<sup>12</sup> Other techniques used in the past to determine  $E_g$  involve a magnetic field: the analysis of the Hall coefficient in the intrinsic region,<sup>8</sup> the determination of the electron effective mass (and then a calculation of  $E_g$  from an  $E(k)$  dispersion relation) by the magnetophonon effect,<sup>13</sup> and magneto-optical methods based upon one-photon interband methods,<sup>4,6,14-16</sup> cyclotron resonance,<sup>17</sup> electron spin resonance,<sup>18</sup> and combined- or cyclotron-phonon resonance.<sup>19</sup> Nonlinear optical methods using four-photon mixing<sup>20</sup> and two-photon absorption (TPA) techniques with a  $\text{CO}_2$  laser<sup>21,22</sup> have also been successfully used to determine  $E_g$ . Recently, it has been shown that TPA methods using a  $\text{CO}_2$  laser can be used to accurately determine  $E_g$  for samples with  $0.24 \leq x \leq 0.30$  by applying external magnetic fields.<sup>23,24</sup>

In this paper we will (1) show how two-photon magnetoabsorption (TPMA) methods are used to determine  $E_g$ , (2) review magneto-optically obtained liquid helium temperature data which, along with our new TPMA values for  $E_g$ , are used to confirm which empirical relationship for  $E_g(x, T)$  most accurately fits the data for the region  $0 \leq x \leq 0.3$ , and (3) present and analyze the nonlinear variation of  $E_g$  with temperature to determine a new functional

relationship that can be used to describe the observed temperature nonlinearities.

## II. EXPERIMENTAL WORK

The experiments reported here were carried out on single crystal, bulk grown samples (both *n*- and *p*-type) with *x* values ranging from  $\approx 0.24$  to 0.30. All samples were polished, etched, and had contacts made with pure indium. A summary of the sample properties is given in Table I. For samples #3–5, the value of *x* and its uncertainty were supplied by Cominco and are tied to *x* values determined by wet chemistry.<sup>25</sup> Sample #1 was supplied by Honeywell with its *x* value derived by infrared cutoff measurements, and sample no. 2 was supplied by Texas Instruments. For sample no. 2 we have determined *x* by first measuring  $E_g$  and then using an  $E_g(x, T)$  relationship.<sup>7</sup> For the purpose of determining the *x* dependence of  $E_g$ , sample no. 2 was not used since *x* was not independently measured.

The monochromatic output of a grating tunable continuous wave (cw) CO<sub>2</sub> laser was focused onto a sample placed in the solenoid of a superconducting magnet capable of producing dc magnetic fields as high as 12 T (or 120 kG). The direction of propagation of the linearly polarized laser light was parallel to the magnetic field, while the samples were mounted in a transverse magnetoresistance geometry. A zero-order wave plate could be used to produce circularly polarized light. Lattice heating effects are important to eliminate since most of the sample properties are temperature dependent. This was accomplished in two ways: (1) the laser beam was mechanically chopped into 20  $\mu$ s wide pulses with a low duty cycle ( $< 1\%$ ), and (2) the beam was significantly attenuated by a commercial attenuator. Photoconductivity (PC) measurements were used to detect and record the small changes in absorption due to weak two-photon magneto-optical transitions. The resulting magneto-optical spectra, obtained by boxcar-averaging techniques, were then recorded on an *x*-*y* recorder.

The sample temperature was measured using a calibrated carbon-glass resistor placed close to the sample. The accuracy of the temperature measurements is estimated to be  $\pm 0.5$  K at low temperatures and about  $\pm 1$  to 2 K at higher temperatures. The calibration constant of the superconducting magnet (tesla/amp) was verified by utilizing the Shubnikov–de Haas (SdH) effect in GaSb samples. The SdH effect is an oscillatory magnetoresistance effect which is periodic in inverse magnetic field and is observable over the entire magnetic field range of the magnet (0.3 to  $> 12$  T). Com-

TABLE I. Sample electrical properties and *x* values.

Sample number	<i>n</i> (77 K) (cm <sup>-3</sup> )	$\mu$ (77 K) (cm <sup>2</sup> /Vs)	<i>x</i> value
1	$1.4 \times 10^{14}$	$1.6 \times 10^5$	0.239
2	$2.8 \times 10^{14}$	$1.2 \times 10^5$	0.253
3	$1.0 \times 10^{14}$	$7.6 \times 10^4$	$0.259 \pm 0.0015$
4	$1.4 \times 10^{14}$	$6.6 \times 10^4$	$0.277 \pm 0.001$
5	$9.9 \times 10^{13}$	$5.3 \times 10^4$	$0.300 \pm 0.0035$

parison of these results with those obtained with a dc electro-magnet (0–2 T) calibrated with nuclear magnetic resonance techniques allowed us to establish a 1% absolute field accuracy.

## III. RESULTS

### A. Determination of $E_g$ by TPMA techniques

In this section of the paper we illustrate how  $E_g$  can be accurately determined from TPMA spectra. Figure 1 shows the PC response versus magnetic field for sample no. 2 for various CO<sub>2</sub> laser wavelengths. As pointed out previously,<sup>23,24</sup> the dominant TPMA structure for HgCdTe alloys consists of two peaks in the PC response caused by two-photon absorption between specific valence band Landau levels and conduction band Landau levels. The TPMA transition energies can be written

$$2\hbar\omega = E_c^{a,b}(n_c, B) - E_v^{a,b}(n_v, B), \quad (1)$$

where  $\hbar\omega$  is the laser photon energy,  $E_c^{a,b}(n_c, B)$  [ $E_v^{a,b}(n_v, B)$ ] represents the energies of the conduction band [valence band] Landau levels in different spin states *a* or *b* as calculated by a modified Pidgeon–Brown band model,<sup>6</sup> *n* is the Landau level number, and *B* is the magnetic field. Polarization studies show that the two peaks arise for the left circularly polarized TPMA transitions  $a^+(-1) \rightarrow a^c(1)$  [ $L_1$  transition, at highest fields and  $n_v = -1$ ,  $n_c = +1$ ] and  $b^+(-1) \rightarrow b^c(1)$  [ $L_2$  transition], where the plus sign

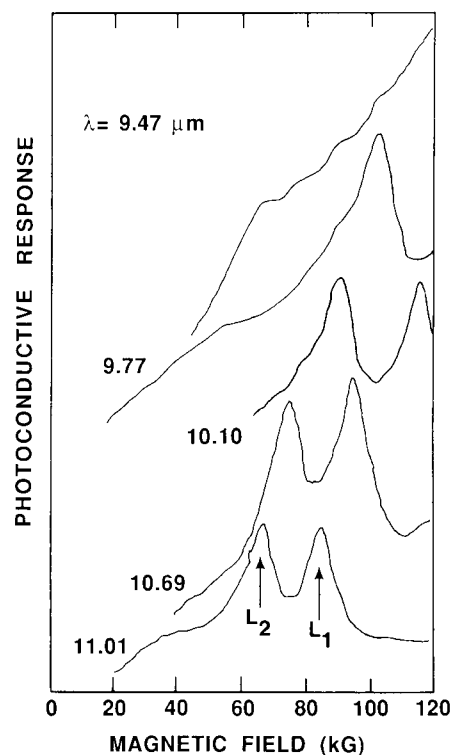


FIG. 1. Photoconductive response of sample no. 2 ( $x = 0.253$ ) for various CO<sub>2</sub> laser wavelengths at 7 K. The two large broad peaks, identified as  $L_1$  and  $L_2$ , arise from resonant two-photon absorption processes identified in the text.

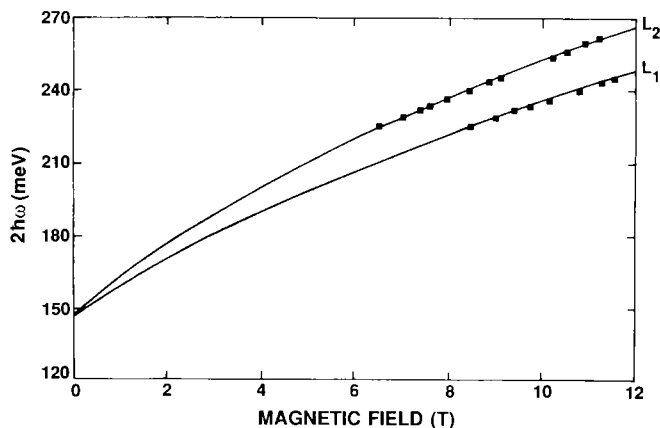


FIG. 2. Two-photon transition energies vs magnetic field for sample no. 2. The solid lines represent the best fit of the transition energies calculated from Eq. (1) to the data giving  $E_g = 146.5 \text{ meV} \pm 1.0 \text{ meV}$ . The data points are restricted by the  $2\hbar\omega$  values that can be obtained from the  $\text{CO}_2$  laser.  $T = 7 \text{ K}$ .

refers to light hole Landau levels. Note that as  $B \rightarrow 0$ ,  $2\hbar\omega \rightarrow E_g$ .

Figure 2 shows a plot of the experimental data shown in Fig. 1 of the values of  $2\hbar\omega$  versus resonant  $B$  field. Theoretical results for the dependence of  $2\hbar\omega$  on  $B$  are calculated from Eq. 1 by using a modified Pidgeon-Brown energy band model.<sup>6</sup> The Landau level energies were calculated by using Weiler's set of band parameters<sup>6</sup>:  $E_p = 19 \text{ eV}$ ,  $\Delta = 1 \text{ eV}$ ,  $\gamma_1 = 3.3$ ,  $\gamma_2 = 0.1$ ,  $\gamma_3 = 0.9$ ,  $\kappa = -0.8$ ,  $F = -0.8$ ,  $q = 0.0$ , and  $N_1 = 0.0$ . The value of  $E_g$  is then easily determined by fitting the theoretical calculations to the data with  $E_g$  as an adjustable parameter. The result for sample no. 2 is  $E_g = 146.5 \pm 1.0 \text{ meV}$  at  $T = 7 \text{ K}$ . These two-photon magneto-optical techniques are the best method for accurately determining the energy gap of a semiconductor in part because resonant optical absorption processes occur between Landau levels. One key advantage of TPMA is that it takes place in the bulk of the sample and is thus much less sensitive to surface preparation than one-photon techniques.

In addition, exciton corrections are much smaller for TPMA than for one-photon absorption and thus do not significantly impact the observed transitions. We note that although samples no. 3–5 are compensated, TPMA effects can still be easily observed and thus used to determine accurate values for  $E_g$ .

### B. Dependence of $E_g(x, T)$ on $x$ value (for $0 \leq x \leq 0.3$ )

A number<sup>1-11</sup> of  $E_g(x, T)$  relationships exist in the literature and various researchers use different ones in their day-to-day applications. No consensus exists as to which actually describes the real variation of  $E_g$  with  $x$ . In this section we show that our TPMA-derived  $E_g$  values verify the Hansen, Schmit, and Casselman (HSC)<sup>7</sup> relationship for  $E_g(x, T)$  ( $0 \leq x \leq 0.3$ ). We also review various  $E_g(x, T)$  relationships<sup>5-7,9,10</sup> and the magneto-optical data<sup>15,16,18-20,26</sup> that can be used as a basis to derive the  $E_g(x, T)$  dependence. Magneto-optical studies have proven capable of accurately deter-

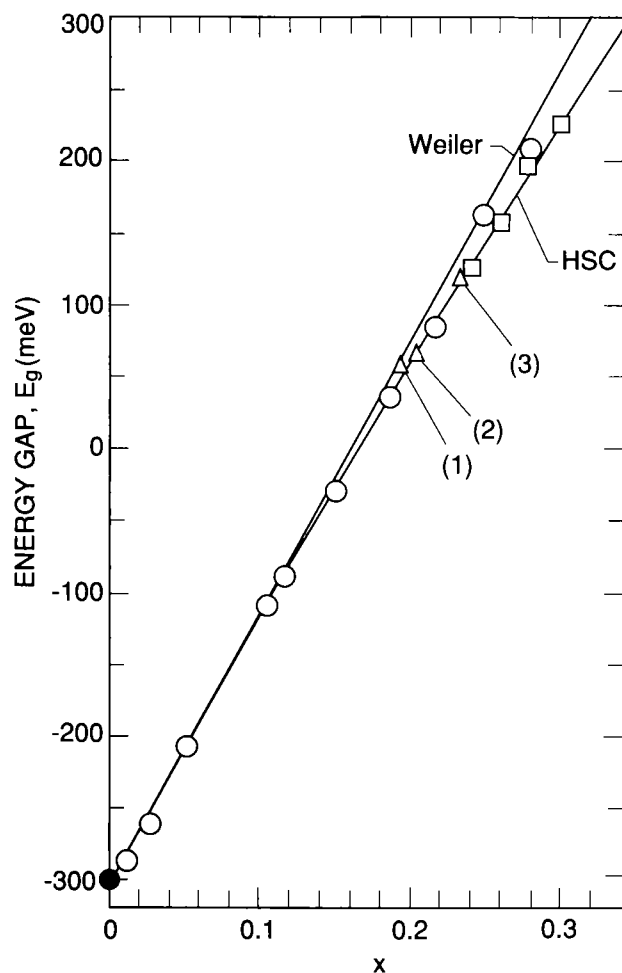


FIG. 3. The low-temperature ( $\approx 4 \text{ K}$ )  $x$  dependence of the energy gap for alloys with  $0 \leq x \leq 0.3$  selected magneto-optical data are presented as identified by the various symbols. The two solid lines represent extremes of the published  $E_g(x, T)$  relationship: Weiler (Ref. 6) and HSC (Ref. 7). ● Ref. 26, IMA; ○ Refs. 15, 16, IMA; △ (1) Ref. 18 ESR; △ (2) Ref. 19, CCCPR; △ (3) Ref. 20, four photon mixing (ESR); □ present work, TPMA.

mining energy band parameters (e.g.,  $E_g$  values) of semiconductors because of the resonant optical transitions that occur between magnetically quantized electronic states. For this reason we concentrate on magneto-optical determinations of  $E_g$ . We note that our calculations of the two-photon transition energies show negligible dependence on the crystallographic orientation of the magnetic field direction because of the particular set of band parameters that describe MCT. Unoriented samples can thus be used because anisotropic effects need not be considered.

Figure 3 shows a plot of  $E_g(x, T)$  for several sets of magneto-optically derived  $E_g$  values for very low temperatures ( $< 10 \text{ K}$ ),<sup>15,16,18-20,26</sup> along with our TPMA-deduced values of  $E_g$ . Table II gives the values of  $E_g$  and  $x$  used in the graphs of Figs. 3 and 4 along with the magneto-optical technique used to obtain them. To the authors' knowledge, these are the most reliable data to use. The variations of two empirical relationships that represent the most extreme behavior are also shown in Fig. 3 by the solid lines (Weiler's<sup>6</sup> and the HSC relationship<sup>7</sup>). It is immediately clear that the biggest differ-

TABLE II. Low temperature magneto-optical derived values of  $E_g(x)$ . Various magneto-optical techniques used include (1) IMA—interband magnetoabsorption, (2) ESR—electron spin resonance, (3) CCCPR—cyclotron, combined and cyclotron phonon resonances, (4) four-photon mixing, and (5) TPMA—two-photon magnetoabsorption. These values are used in Fig. 3 and/or Fig. 4.

$x$ value	$E_g$ (meV)	Magneto-optical technique used	Reference	Comments
0	$-299.7 \pm 0.5$	IMA	26	at 8 K
0.01	-285	IMA	15,16	at 4 K
0.025	-261			
0.05	-207			
0.105	-110			
0.115	-90			
0.15	-30			
0.185	35			
0.215	86			
0.25	161			
0.28	208			
0.193	56	ESR	18	at 4 K
0.203	$64 \pm 3$	CCCPR	19	at 4 K
0.234	119	Four-photon mixing (ESR)	20	at 4 K
0.239	$122 \pm 1$	TPMA	present work	at 2–10 K
$0.259 \pm 0.0015$	$158.5 \pm 1$			
$0.277 \pm 0.001$	$195 \pm 1$			
$0.300 \pm 0.0035$	$224 \pm 2$			

ences in these two relationships occur in the 0.2–0.3  $x$ -value region. Thus, in order to test which relationship is most accurate, we replot the magneto-optical data in the range 0.2–0.3 in Fig. 4. For completeness we also include the variations of three additional empirical relationships that have also been reported in the literature: Nemirovsky and Finkman (NF),<sup>5</sup> Chu, Xu, and Tang (CXT),<sup>9</sup> and Legros and Triboulet (LT).<sup>10</sup> In addition we have added two values from the recent EMIS Datareviews Series No. 3.<sup>11</sup> The Schmit and Stelzer<sup>3</sup> relationship was not included because the low value of  $E_g$  ( $-250$  meV) obtained from it at  $x = 0$  is in major disagreement with the low  $x$ -value MCT data of Guldner *et al.*<sup>15,16</sup> and the HgTe results from Dobrowolska *et al.*<sup>26</sup> The extremely wide variation in predicted  $E_g$  values from these relationships is apparent. The important observation to note is that the present TPMA work verifies the use of the HSC relationship as representing the best value of  $E_g(x, T)$  in the range 0.0–0.3 at very low temperatures ( $< 10$  K). Unless the good fit is fortuitous, it implies the validity of the gap determination using detector cutoff energy and  $\alpha = 500 \text{ cm}^{-1}$  absorption edge data.

### C. Dependence of $E_g$ on $T$ (for $0.24 < x < 0.26$ )

Most workers have ignored the fact the  $E_g(T)$  should vary nonlinearly with  $T$  at low temperatures (see the thermodynamic arguments presented later). Accurate low tem-

perature  $E_g(T)$  data simply did not exist. Now, however, the accuracy of determining  $E_g(T)$  by TPMA techniques allows an empirical expression for  $E_g(T)$  to be determined. Figure 5 shows how the TPMA spectra obtained at  $\lambda = 10.24 \mu\text{m}$  depend upon lattice temperature  $T$ . A shift in magnetic field positions of the resonant  $L_1$  and  $L_2$  structure is seen to be small for  $T \leq 15$  K, but quite noticeable for  $T > 15$  K. The shift of the resonant structure to lower magnetic fields for increasing temperatures is a direct consequence of the increasing energy gap, since as  $E_g$  becomes larger, the valence and conduction band Landau levels become further apart in energy. Thus, smaller values of magnetic field are required to meet the TPMA resonant condition for a given two-photon energy. At each temperature, multiple wavelengths were then used to determine values of  $E_g$  in the manner described in Sec. III A.

We propose to replace the linear temperature term  $T$  in the HSC relation by the term  $(A + T^3)/(B + T^2)$ . This functional relationship agrees with the HSC relationship at high temperatures, while allowing for an offset from the HSC relationship at 0 K. It also agrees with the fact that  $dE_g/dT = 0$  at 0 K. The size of the 0 K offset is determined by  $A/B$ , while the temperature above which agreement with HSC occurs is determined from the inequalities  $T \gg \sqrt[3]{A}$  and  $T \gg \sqrt{B}$ .

We have simultaneously fitted a composite of three sets of  $E_g$  versus  $T$  data for the samples with  $x = 0.239$ ,  $x = 0.253$ ,

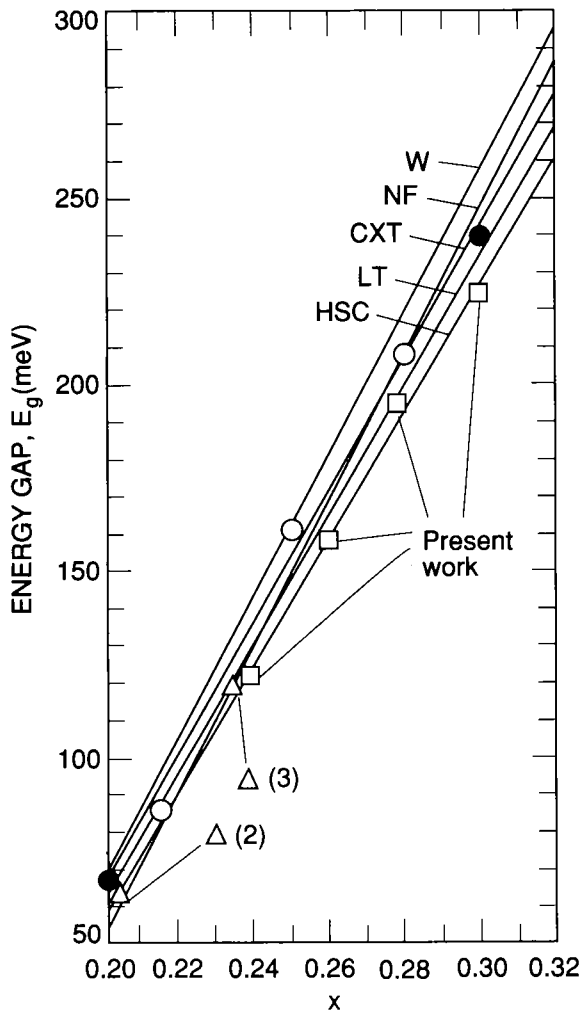


FIG. 4. The low-temperature ( $\approx 4$  K)  $x$ -dependence of the energy gap for  $0.2 \leq x \leq 0.3$ . This is the most technologically interesting region for infrared detectors and is the region where the various  $E_g(x, T)$  relationships differ the most. Again, various magneto-optical data are presented as well as the numbers given in the recent EMIS Databooks Series (Ref. 11). The solid lines represent various published relationships describing  $E_g(x, T)$ : W (Ref. 6), NF (Ref. 5), CXT (Ref. 9), LT (Ref. 10), and HSC (Ref. 7). Note that the TPMA data from the present work agrees best with the HSC relationship.  $\circ$  Refs. 15 and 16;  $\bullet$  EMIS Databooks Series no. 3 (1987).

and  $x = 0.259$  by the nonlinearly least squares routine contained in DATAPLOT.<sup>27</sup> The first and third values were obtained from Cominco, while the second was chosen to be consistent with the HSC relationship at high temperatures.

Our data merge smoothly with the HSC relationship above 100 K. Below 100 K the data lie below the HSC relationship, and become constant before 10 K. Figure 6 shows the composite data rationalized for comparison by subtracting the 0 K energy gap obtained from HSC and dividing by  $0.535(1 - 2x)$ . Rationalized HSC values are used at high temperature so that a fit was obtained between 0 and 300 K. The constants  $A$  and  $B$  that best fit all the data are:  $A = -1822 \text{ K}^3$  and  $B = 255.2 \text{ K}^2$ . Although  $A$  and  $B$  can vary with  $x$ , no trend was observed by fitting the data individually for each sample, and thus we obtain the  $A$  and  $B$  values which best fit all the data. The offsets between our fit

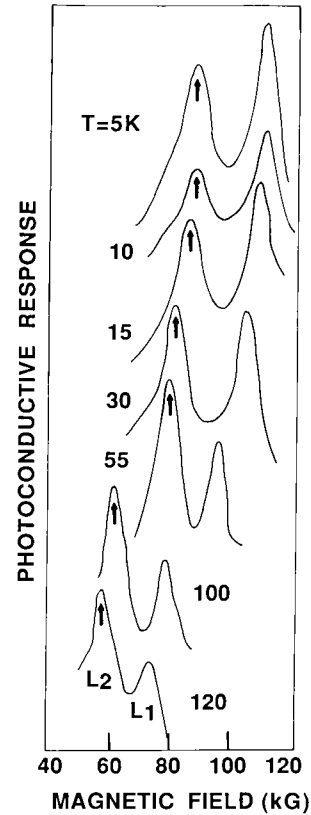
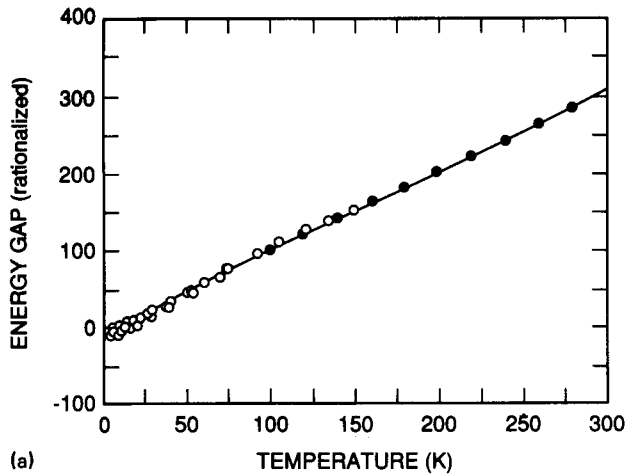


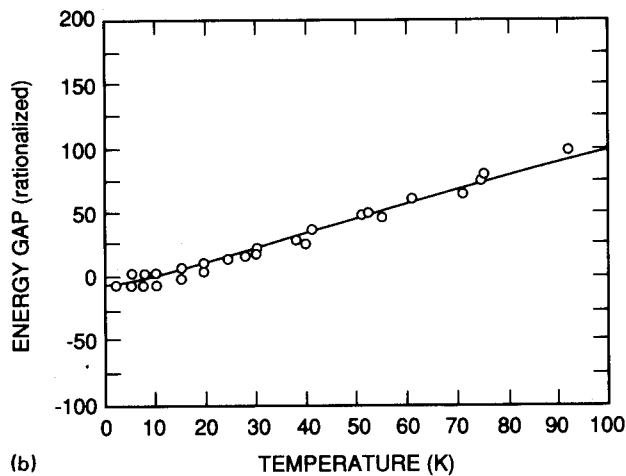
FIG. 5. Temperature dependence of the photoconductive TPMA spectra for sample no. 2. Note the (1) TPMA structure can clearly be seen up to 120 K and beyond, and (2) the peaks do not shift with temperature from 5 to 10 K.  $\lambda = 10.24 \mu\text{m}$ .

and HSC at 0 K are on the order of 2 meV, which is comparable to the value implied by the uncertainty in  $x$  values. Even though at 0 K the offsets are small, the differences predicted by our new relationship and associated with the nonlinear temperature dependence of  $E_g$  are on the order of 3–4 meV at 10–12 K and should be taken into account in experiments requiring high accuracy.

Figures 7(a)–(c) show the data for the energy gap as a function of temperature for each sample along with the result of the composite fit. In each case the fit is adequate relative to the  $\pm 2$  meV uncertainty that arises mainly from the uncertainty in  $x$ . Figure 8(a) shows  $dE_g/dT$ , rationalized as in Fig. 6, determined from the data as well as the fit (represented by the line). It is seen that  $dE_g/dT$  rises rapidly at low temperatures, reaches a peak at 10–12 K, and then becomes asymptotic to that of HSC. A peak was predicted by Popko and Pawlikowski<sup>28</sup> from the dilatational part of the temperature dependence of the energy gap. We have revised their calculations by using more recent data obtained by Caporaletti and Graham<sup>29</sup> for the thermal expansion coefficient of  $\text{Hg}_{1-x}\text{Cd}_x\text{Te}$  alloys. We have obtained the value for  $x = 0.25$  alloys by averaging the values obtained at 0.20 and 0.30 in Ref. 29. The 25% rise in  $dE_g/dT$  above unity at 10–12 K seen in Fig. 8(a) is found to agree numerically when the new expansion coefficient value is used in the formula of Ref. 28. Figure 8(b) shows the difference between our new



(a)



(b)

FIG. 6. (a) Rationalized energy gaps as a function of temperature for (○) samples nos. 1 ( $x = 0.239$ ), 2 ( $x = 0.253$ ), and 3 ( $x = 0.259$ ); (●) with HSC at high temp and fit. Rationalized values from HSC are used at temperatures above those reached by the data. Fit by the expression  $(A + T^3)/(B + T^2)$  is the solid line. (b) An expansion of (a) between 0 and 100 K. Sample nos. 1–3 and fit.

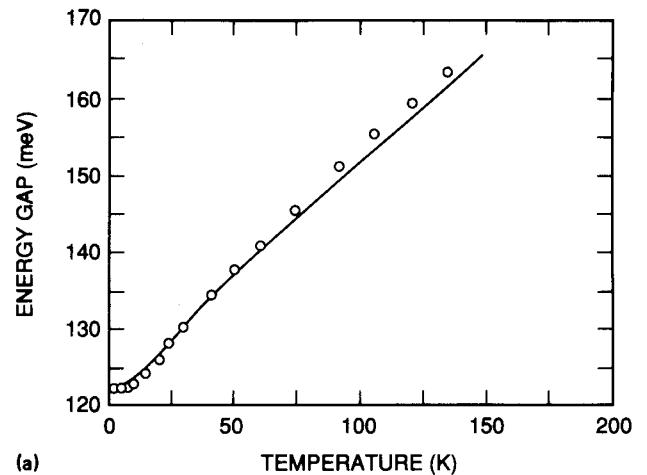
relationship and that of HSC as a function of temperature for  $x = 0.2, 0.25$ , and  $0.3$ . The difference peaks near 10–12 K and becomes negligible above 100 K for each curve.

According to the laws of thermodynamics discussed by Thurmond,<sup>30</sup> the forbidden energy gap,  $\Delta E_{cv}$ , is the standard Gibbs energy for formation of electrons and holes as a function of temperature. The temperature dependence of  $\Delta E_{cv}$  may be found from the standard thermodynamic relations<sup>31</sup>:

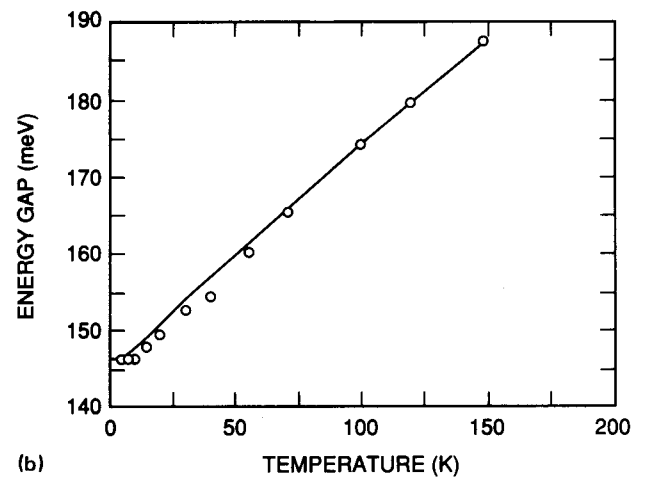
$$\begin{aligned} d(\Delta E_{cv}) &= d(\Delta H_{cv}) - Td(\Delta S_{cv}) - dT(\Delta S_{cv}) \\ &= Td(\Delta S_{cv}) + (\Delta V_{cv})dp - Td(\Delta S_{cv}) \\ &\quad - dT(\Delta S_{cv}) \\ &= (\Delta V_{cv})dp - dT(\Delta S_{cv}), \end{aligned}$$

$$d(\Delta E_{cv})/dT = -\Delta S_{cv} \text{ if } dp = 0 \text{ (fixed pressure)}$$

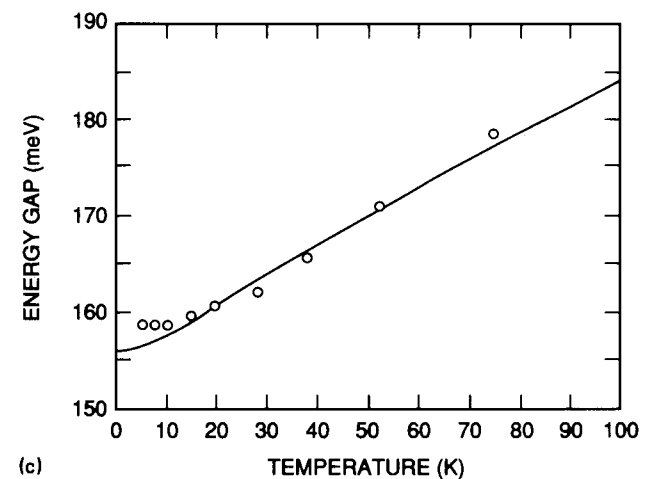
where  $\Delta H_{cv}$  is the enthalpy of formation,  $\Delta S_{cv}$  is the entropy of formation,  $\Delta V_{cv}$  is the volume change,  $T$  is temperature, and  $p$  is pressure. By the third law of thermodynamics,  $\Delta S_{cv} \rightarrow 0$  as  $T \rightarrow 0$ , so that  $d(\Delta E_{cv})/dT \rightarrow 0$  as  $T \rightarrow 0$ . The en-



(a)



(b)



(c)

FIG. 7. (a) Energy gaps of sample #1 ( $x = 0.239$ ) as a function of temperature. The fit by our new relationship is the solid line. (b) Same as (a) for sample no. 2 ( $x = 0.253$ ). (c) Same as (a) for sample no. 3 ( $x = 0.259$ ).

trophy in this case goes to zero physically because all valence states become filled and all conduction states become empty. It is mathematically satisfying that the derivative becomes zero because there is no temperature below absolute zero,

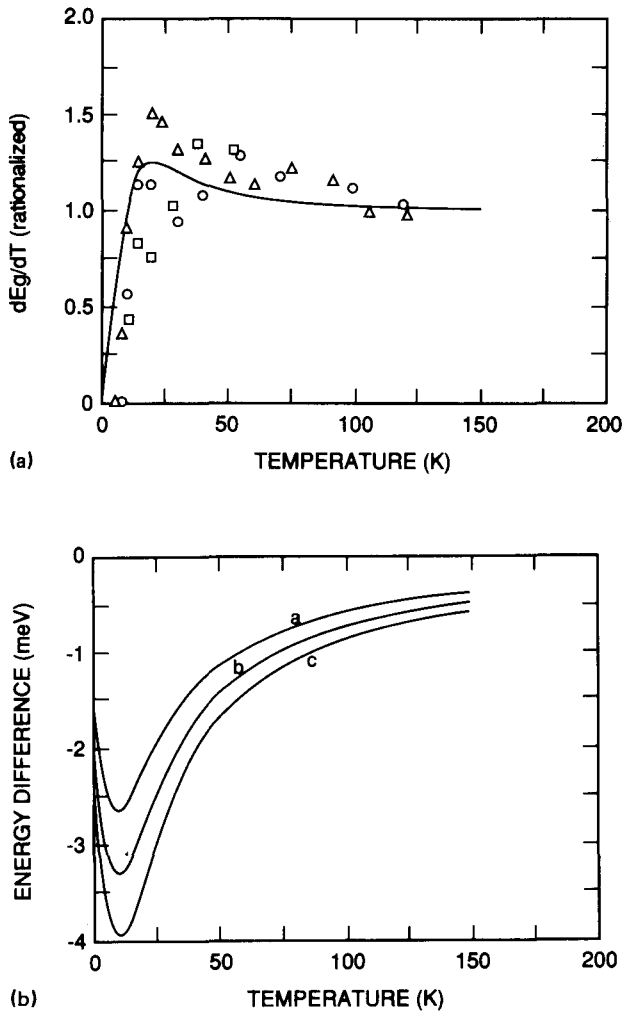


FIG. 8. (a) Rationalized derivative of the energy gap with temperature as a function of temperature for the data of samples nos. 1 ( $\Delta$ ), 2 ( $\circ$ ), and 3 ( $\square$ ) ( $x=0.239$ ,  $0.253$ , and  $0.259$ ) along with that corresponding to the fit,  $(A + T^3)/(B + T^2)$ . (b) Difference in energy between our relation and HSC as a function of temperature for  $x =$  (a) 0.3, (b) 0.25, and (c) 0.2.

which would be needed in the definition of the derivative if it were finite.

#### IV. SUMMARY AND CONCLUSIONS

Accurate determinations of the energy gap by two-photon magnetoabsorption techniques at liquid helium temperatures in alloys of  $0.24 \leq x \leq 0.30$  have been made. They are shown to help verify the use of the Hansen-Schmit-Casselmann relation, one of many existing, over the range  $0 < x < 0.30$  at these temperatures. In contrast, the observed temperature dependence is nonlinear and thus cannot be described accurately (better than 3–4 meV) by the HSC relation below 77 K. Analysis of  $E_g(T)$  data for three samples with  $0.24 \leq x \leq 0.26$  has allowed the deduction of a new relationship for  $E_g(x, T)$  that more properly accounts for the nonlinear temperature dependence below 77 K and the nearly linear behavior above 77 K

$$E_g(x, T) = -0.302 + 1.93x + 5.35(1 - 2x)(10^{-4}) \\ \times [(-1822 + T^3)/(255.2 + T^2)] \\ - 0.810x^2 + 0.832x^3,$$

for  $E_g$  in eV and  $T$  in K.

This relation should apply to alloys with  $0.2 < x < 0.3$ .

For samples with  $10 \mu\text{m}$  cutoff wavelengths (i.e.,  $x \approx 0.2$ ), the maximum deviation of our new relation from that of HSC is approximately 3–4 meV at  $\sim 10$ –12 K. At lower temperatures,  $E_g$  becomes independent of  $T$  and for higher temperatures the difference grows smaller, finally becoming negligible at temperatures over 100 K. The major reason for the observed nonlinear behavior of  $E_g$  seems to be related to (1) the dilatational part of  $E_g$  as predicted earlier by Popko and Pawlikowski and (2) the fact that  $dE_g/dT$  must go to zero at  $T = 0$  K as predicted by the third law of thermodynamics.

The work in this paper on the nonlinear temperature dependence of  $E_g$  at  $T < 77$  K is also significant because it provides valuable input for the proper interpretation of low temperature photoluminescence (PL) spectra. For example, low temperature PL spectra for alloys with  $x \approx 0.3$  are often composed of multiple lines attributed to recombination originating from band-to-band, band-to-acceptor, donor-to-acceptor, and/or bound exciton transitions.<sup>12,32,33</sup> The identification and interpretation of each particular PL line is usually made by determining the variation in intensity of the line with pump power and the shift in the line energy with lattice temperature. The energy of the PL lines usually shift with temperature and those shifts are then compared with the shifts in band gap energy with temperature. Consequently, accurate knowledge of the nonlinear temperature variation of  $E_g$  for  $T < 77$  K is important.

#### ACKNOWLEDGMENTS

We acknowledge the partial support of this work at UNT by the U.S. Army Center for Night Vision and Electro-Optics, Contract No. DAA B07-87-C-F094. Regarding Cominco, Honeywell, and Texas Instruments, reference to material obtained is included for completeness of exposition and constitutes neither an endorsement by NIST nor representation that the material referenced is the best available for the purpose.

<sup>1</sup>J. D. Wiley and R.N. Dexter, Phys. Rev. **181**, 1181 (1969).

<sup>2</sup>M. W. Scott, J. Appl. Phys. **40**, 4077 (1969).

<sup>3</sup>J. L. Schmit and E. L. Stelzer, J. Appl. Phys. **40**, 4865 (1969).

<sup>4</sup>M. H. Weiler, R. L. Aggarwal, and B. Lax, Phys. Rev. B **16**, 3603 (1977).

<sup>5</sup>Y. Nemirovsky and E. Finkman, J. Appl. Phys. **50**, 8107 (1979).

<sup>6</sup>M. H. Weiler, in *Semiconductor and Semimetals*, edited by R. K. Willardson and A. C. Beer (Academic, New York, 1981) Vol. 16, p. 119.

<sup>7</sup>G. L. Hansen, J. L. Schmit, and T. N. Casselman, J. Appl. Phys. **53**, 7099 (1982).

<sup>8</sup>E. Finkman, J. Appl. Phys. **54**, 1883 (1983).

<sup>9</sup>J. Chu, S. Xu, and D. Tang, Appl. Phys. Lett. **43**, 1064 (1983).

<sup>10</sup>R. Legros and R. Triboulet, J. Crystal Growth **72**, 264 (1985).

<sup>11</sup>J. C. Brice, in *EMIS Datareviews Series*, No. 3 (INSPEC, London, 1987), p. 103.

<sup>12</sup>See, for example, A. T. Hunter and T. C. McGill, J. Appl. Phys. **52**, 5779 (1981).

- <sup>13</sup>See, for example, S. W. McClure, D. G. Seiler, C. L. Littler, and M. W. Goodwin, *J. Vac. Sci. Technol. A* **3**, 271 (1985).
- <sup>14</sup>S. H. Groves, T. C. Harman, and C. R. Pidgeon, *Solid State Commun.* **9**, 451 (1971).
- <sup>15</sup>Y. Guldner, C. Rigaux, A. Mycielski, and Y. Couder, *Phys. Status Solidi B* **81**, 615 (1977).
- <sup>16</sup>Y. Guldner, C. Rigaux, A. Mycielski, and Y. Couder, *Phys. Status Solidi B* **82**, 149 (1977).
- <sup>17</sup>T. O. Poehler and J. R. Apel, *Phys. Lett.* **32A**, 268 (1970).
- <sup>18</sup>B. D. McCombe, R. J. Wagner, and G. A. Prinz, *Phys. Rev. Lett.* **25**, 87 (1970).
- <sup>19</sup>B. D. McCombe, R. J. Wagner, and G. A. Prinz, *Solid State Commun.* **8**, 1687 (1970).
- <sup>20</sup>T. J. Bridges, E. G. Burkhardt, and V. T. Nguyen, *Optics Commun.* **30**, 66 (1979).
- <sup>21</sup>D. G. Seiler, S. W. McClure, R. J. Justice, M. R. Loloee, and D. A. Nelson, *Appl. Phys. Lett.* **48**, 1159 (1986).
- <sup>22</sup>D. G. Seiler, S. W. McClure, R. J. Justice, M. R. Loloee, and D. A. Nelson, *J. Vac. Sci. Technol. A* **4**, 2034 (1986).
- <sup>23</sup>D. G. Seiler, C. L. Littler, M. R. Loloee, and S. A. Milazzo, *J. Vac. Sci. Technol. A* **7**, 370 (1989).
- <sup>24</sup>D. G. Seiler, M. R. Loloee, S. A. Milazzo, A. J. Durkin, and C. L. Littler, *Solid State Commun.* **69**, 757 (1989).
- <sup>25</sup>W. F. H. Micklethwaite, *J. Appl. Phys.* **63**, 2382 (1988).
- <sup>26</sup>M. Dobrowolska, A. Mycielski, and W. Dobrowolski, *Solid State Commun.* **27**, 1233 (1978).
- <sup>27</sup>DATAFLOW is a software package developed at NIST (formerly NBS) for analyzing and displaying data; see *DATAFLOW—Introduction and Overview*, NBS Special Publication 667 (U.S. GPO, Washington, D. C., 1984).
- <sup>28</sup>E. Popko and J. M. Pawlikowski, *Phys. Status Solidi A* **46**, K9 (1978).
- <sup>29</sup>O. Caporaletti and G. M. Graham, *Appl. Phys. Lett.* **39**, 338 (1981).
- <sup>30</sup>C. D. Thurmond, *J. Electrochem. Soc.* **122**, 1133 (1975).
- <sup>31</sup>J. Reif, in *Fundamentals of Statistical and Thermal Physics* (McGraw-Hill, New York, 1965).
- <sup>32</sup>A. T. Hunter, D. L. Smith, and T. C. McGill, *Appl. Phys. Lett.* **37**, 200 (1980).
- <sup>33</sup>B. L. Gel'mont, V.I. Ivanov-Omskii, V.A. Mal'tseva, and V.A. Smirnov, *Sov. Phys. Semicond.* **15**, 638 (1981).